Revealing the Orbital Origins of Exotic Electronic States with Ti Substitution in Kagome Superconductor CsV_3Sb_5

Zihao Huang,[1,2,*] Hui Chen,[1,2,*,†] Hengxin Tan,[3,*] Xianghe Han,[1,2] Yuhan Ye,[1,2] Bin Hu,[1,2] Zhen Zhao,[1,2] Chengmin Shen,[1,2] Haitao Yang,[1,2] Binghai Yan,[3,‡] Ziqiang Wang,[4] Feng Liu,[5] and Hong-Jun Gao[1,2,§]

[1]*Beijing National Center for Condensed Matter Physics and Institute of Physics, Chinese Academy of Sciences, Beijing 100190, China*
[2]*School of Physical Sciences, University of Chinese Academy of Sciences, Beijing 100190, China*
[3]*Department of Condensed Matter Physics, Weizmann Institute of Science, Rehovot, Israel*
[4]*Department of Physics, Boston College, Chestnut Hill, Massachusetts 02467, USA*
[5]*Department of Materials Science and Engineering, University of Utah, Salt Lake City, Utah 84112, USA*

(Received 19 June 2024; revised 26 November 2024; accepted 23 December 2024; published 4 February 2025)

The multiband kagome superconductor CsV_3Sb_5 exhibits complex orbital textures on the Fermi surface, making the orbital origins of its cascade of correlated electronic states and superconductivity a major scientific puzzle. Chemical doping of the kagome plane can simultaneously tune the exotic states and the Fermi-surface orbital texture and thus offers a unique opportunity to correlate the given states with specific orbitals. In this Letter, by substituting V atoms with Ti in the kagome superconductor CsV_3Sb_5, we reveal the orbital origin of a cascade of its correlated electronic states through the orbital-resolved quasiparticle interference. We analyze the quasiparticle interference changes associated with different orbitals, aided by first-principles calculations. We have observed that the in-plane and out-of-plane vanadium $3d$ orbitals cooperate to form unidirectional coherent states in pristine CsV_3Sb_5, whereas the out-of-plane component disappears with doping-induced suppression of charge density wave and global electronic nematicity. In addition, the Sb p_z orbital plays an important role in both the pseudogap and superconducting states in CsV_3Sb_5. Our findings offer new insights into multiorbital physics in quantum materials that are generally manifested with intriguing correlations between atomic orbitals and symmetry-encoded correlated electronic states.

DOI: 10.1103/PhysRevLett.134.056001

The orbital is a key degree of freedom in quantum materials, where multiple atomic orbitals contribute to their symmetry-breaking low-energy physics and unique properties [1–7]. Strongly correlated materials with complex orbital textures at the Fermi surface (FS) exhibit intriguing orbital-dependent phenomena, such as orbital-dependent band renormalization [8,9], symmetry-breaking states [10,11], and orbital-selective Mott transition [12] and Cooper pairing [13]. Understanding the orbital nature of electronic states is thus essential for uncovering the mechanisms behind these phenomena.

The newly discovered kagome superconductor AV_3Sb_5 ($A = \mathrm{K}$, Rb, Cs) is a multiband superconductor with complex orbital textures at the Fermi level, exhibiting a cascade of correlated electronic states, such as Z_2 topology [14–16], rotation-symmetry-breaking charge density waves (CDWs) [17–20], time-reversal symmetry-breaking states [21–24], pair density waves (PDWs) [25], and electronic nematicity [26–28]. Also, AV_3Sb_5 has been found to exhibit rich orbital-dependent physics [29–32]. Specifically, the anisotropy of the Knight shift in nuclear magnetic resonance measurements of CsV_3Sb_5 indicates possible orbital ordering and fluctuations [33]. The orbital-dependent carrier-doping effect is observed by doping electrons into the surface of CsV_3Sb_5 [34]. The CDW gap opens at the FS of the V d orbital while leaving the Sb orbital intact [35,36], likely due to the FS instabilities of multiple Van Hove singularities from distinct V orbital-derived bands [37,38]. Additionally, it exhibits possible multiband superconductivity [39,40], with the Sb p_z orbital making seemly important contributions [41,42]. However, our fundamental understanding of multiple orbital physics in the AV_3Sb_5 kagome system is still far from complete, especially since the orbital origins of different exotic electronic states remain largely unknown. This is mainly caused by a complex multiorbital FS [32,35,36,38] and the existence of multiple intertwined states [18,26,28,43], which make it difficult to correlate the former with the latter one by one.

Recently, chemically doped AV_3Sb_5 kagome systems have been demonstrated to effectively tune the multiple electronic states [40,42,44,45]. Meantime, the chemical

*These authors contributed equally to this work.
†Contact author: hchenn04@iphy.ac.cn
‡Contact author: binghai.yan@weizmann.ac.il
§Contact author: hjgao@iphy.ac.cn

 © 2025 American Physical Society

doping is expected to also change the orbital textures at the FS. Therefore, we are motivated to investigate the evolution of Fermi-surface orbital textures along with disentangling the cascade of correlated states at different doping levels so that the correlation between the two can be resolved. In this Letter, we systematically substitute V with Ti in the kagome superconductor CsV_3Sb_5, and perform the orbital-resolved quasiparticle interference (QPI) measurements at low temperatures. We have revealed the orbital origins of all the observed quantum states, state by state and orbital by orbital, by analyzing the QPI spectra in combination with scanning tunneling microscopy and spectroscopy, aided with density-functional theory (DFT) calculations (details in Supplemental Material [46]).

The CsV_3Sb_5 single crystal displays a stacking sequence of Cs-Sb2-VSb1-Sb2-Cs layers with hexagonal symmetry (space group No. 191, $P6/mmm$) [Figs. S1(a),(b) [46]]. Within the VSb1 layer, the kagome lattice of V is coordinated by Sb1 atoms at the center of the hexagons, forming a hexagonal lattice [25]. Upon Ti doping, the Ti dopants substitute V sites within the kagome layer [44]. The primary cleavage planes are the Cs and Sb2 planes (Fig. S1 [46]). On the Sb2 planes of $CsV_{3-x}Ti_xSb_5$, there are randomly distributed dark spots that correspond to the Ti dopants in the underlying VSb1 kagome layer [44].

The substitution of V with Ti effectively tunes the cascade of exotic electronic states [24–26,28,43,44,52] in CsV_3Sb_5. The significant differences between the pristine and highly doped phases are directly observable through dI/dV spectra and maps. The long-range 2×2 CDW and $4a_0$ charge stripes [Figs. 1(a) and 1(b)] are significantly suppressed by Ti doping [44], changing into short-range stripes at $x = 0.15$ [Figs. 1(d) and 1(e)]. The cascade of energy scales associated with various electronic orders is examined in averaged tunneling conductance spectra. The CDW gap [18,35] of around 20 meV observed in pristine CsV_3Sb_5 [Fig. 1(c)] persists as a gaplike feature in the Ti-doped sample [Fig. 1(f)] despite suppressed long-range CDWs. The gap of Ti-doped samples, also detected in photoemission spectroscopy and optical measurements [52], may originate from a hidden electronic order, whose onset temperature linked to a muon depolarization anomaly present in both undoped and $x = 0.15$ doped compounds. At lower energies, a smaller gap emerges below ~20 K in CsV_3Sb_5 around 5 meV [orange dotted lines in Fig. 1(c)], identified as a pseudogap from the PDW [25]. This pseudogap weakens but remains visible in the Ti-doped sample, indicating a transition to a short-range PDW. The gap maps further support the Ti-doping-induced suppression of long-range PDWs [Figs. S2(c),(d) [46]]. Below the superconducting (SC) transition temperature T_c, Ti substitution transforms the V-shaped SC gap with residual zero-energy conductance in the pristine [inset of Fig. 1(c)] and lightly-doped phase into a U-shaped SC gap without residual zero-energy conductance in highly doped phase [inset of Fig. 1(f)]. It should be noted that the descriptions of V-shaped or U-shaped gaps are based on residual zero-energy conductance at 0.4 K without making definitive conclusions about the nodal or nodeless nature of the gap function [25,39,53].

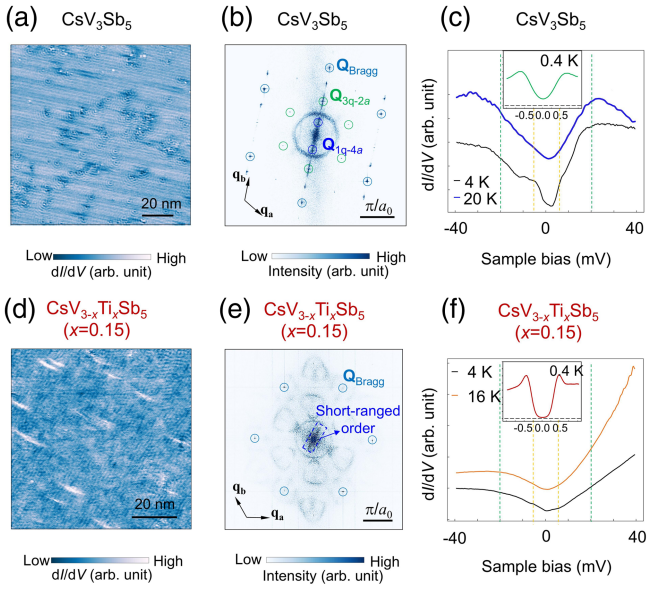

FIG. 1. (a),(b) $dI/dV(\boldsymbol{r}, -50\ \mathrm{mV})$ (a) and corresponding Fourier transform (FT) image (b) of pristine CsV_3Sb_5 (c) dI/dV spectra of CsV_3Sb_5 acquired at 4 K and 20 K, respectively. Inset shows a V-shape SC gap measured at 0.4 K. (d),(e) $dI/dV(\boldsymbol{r}, -20\ \mathrm{mV})$ (d) and corresponding FT image (e) of $CsV_{3-x}Ti_xSb_5 (x = 0.15)$. (f) dI/dV spectra of $CsV_{3-x}Ti_xSb_5 (x = 0.15)$ at 4 K and 16 K. Inset shows the U-shape SC gap measured at 0.4 K.

To investigate the orbital origins of these exotic electronic states, we apply QPI imaging, a powerful technique for determining the orbital features of electronic structures in correlated materials [10,14]. We first examine theoretical results for CsV_3Sb_5. The calculated FS at $k_z = \pi$ mainly comprises three sheets [Fig. 2(a)] stemming from different orbitals: Sb-p_z orbitals (blue), V out-of-plane d_{xz} and d_{yz} orbitals (green), and V in-plane d_{xy} and $d_{x^2-y^2}$ orbitals (red). We perform orbital-resolved QPI simulation [Fig. 2(b)] by considering the scattering vectors within distinct orbital subbands in the constant-energy contour (CEC) [Fig. 2(a)] of the calculated bulk bands (see details in Supplemental Material [46]). Then we compare experimental QPI patterns with theoretical ones. The dI/dV maps $[dI/dV(\mathbf{r}, V)]$ and corresponding Fourier transform (FT) reveal three types of vectors: (1) nondispersive wave vectors of the long-range 2×2 CDW and 1×4 charge stripes [18,25,54,55] (Fig. S3 [46]); (2) a circular QPI pattern that indicates an isotropic scattering vector $\mathbf{q_1}$ [18], primarily from Sb p_z orbitals [Figs. S3 [46] and Fig. 2(b)]; and (3) complex scattering wave vectors that are dominated by V d orbitals near the Fermi level, i.e., $dI/dV\ (\boldsymbol{q}, -5\ \mathrm{mV})$ [Figs. 2(c) and 2(b)].

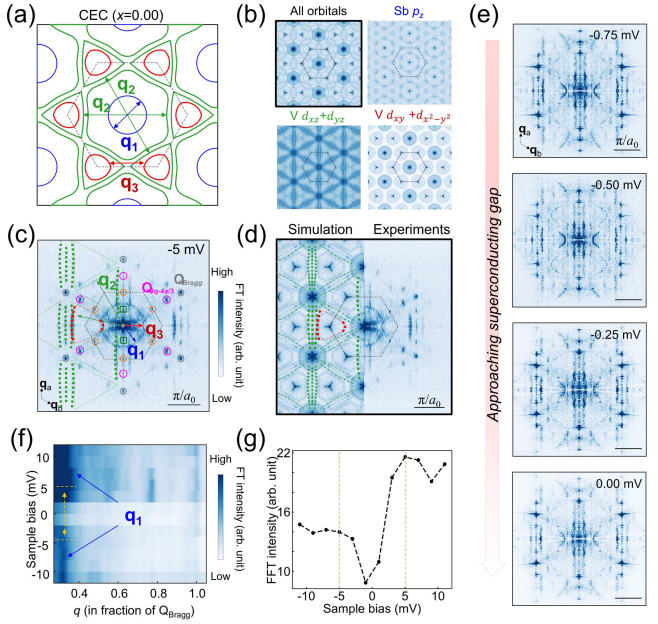

FIG. 2. (a) Calculated Fermi surface of pristine CsV_3Sb_5. The Sb p_z orbital and V out-of-plane d_{xz} and d_{yz} and in-plane $d_{xy} + d_{x^2-y^2}$ orbitals are highlighted by the blue, green, and red colors, respectively. (b) The simulated QPI patterns based on all the orbitals, Sb p_z orbital, V d_{xz} and d_{yz} orbitals, and V $d_{xy} + d_{x^2-y^2}$ orbitals in CEC of (a). (c) FT of dI/dV map in the normal state of CsV_3Sb_5 at -5 mV. (d) The measured -5 mV QPI patterns (right) and the simulated all orbitals QPI pattern (left). (e) The FT of dI/dV map in the superconducting state of CsV_3Sb_5. (f) Radially averaged line cut in FTs of dI/dV maps. (g) Energy-dependent FT intensity of scattering vectors $\mathbf{q_1}$. The FT intensity is the average of 6 pixels in $\mathbf{q}$ space at $\mathbf{q_1}$.

Figure 2(c) reveals complex patterns with unidirectional patches parallel to the 1×4 charge order ($\mathbf{q_2}$, green dashed lines) and broken triangles with arcs perpendicular to the 1×4 charge order ($\mathbf{q_3}$, red dashed triangles). These patches are visible between the energies of ± 12 mV and disappear around 35 K, reported as coherent quasiparticles in symmetry-broken electronic states [17,28]. Comparing with calculations [Fig. 2(d)], $\mathbf{q_2}$ is attributed to scattering of out-of-plane V d_{xz} and d_{yz} orbitals, with energy-dependent dispersion shown in Fig. S4 [46], while $\mathbf{q_3}$ stems from the scattering of in-plane V d_{xy} and $d_{x^2-y^2}$ orbitals [Fig. 2(b)]. The C_2 symmetry in the V in-plane orbital has been reported with evidence of unidirectional electron-phonon coupling in the nematic state [56]. This indicates that electronic states from both V out-of-plane and in-plane orbitals exhibit unidirectionality, breaking the crystalline symmetry into C_2 symmetry.

In the superconducting states, the low-energy QPIs are dominated by Bogoliubov quasiparticles as the energy approaches the superconducting gap [Fig. 2(e)]. The FTs of dI/dV maps show $\mathbf{q_2}$ and $\mathbf{q_3}$ QPIs [Fig. 2(e)] at the energy both beyond and within the V-shape gap [25], consistent with the finite zero-energy density of states. Additionally, the $\mathbf{q_3}$ arcs alongside the unidirectional patches $\mathbf{q_2}$ become clearer, also showing C_2 symmetry. Notably, the circular pattern from Sb p_z orbitals $\mathbf{q_1}$ fades and disappears below 5 mV [Fig. 2(e) and Fig. S5 [46]], coinciding with the pseudogap observed [Fig. 1(c)] in CsV_3Sb_5. A radially averaged line cut in FTs of dI/dV maps demonstrates the evolution of $\mathbf{q_1}$ in the -11 mV–11 mV range [Fig. 2(f)], with suppressed intensity within the -5 mV–5 mV pseudogap. The energy-dependent FT intensity clearly reveals a pseudogap feature [Fig. 2(g)]. The absence of $\mathbf{q_1}$ within the pseudogap and SC gap energy ranges suggests its significant contribution to their formation.

Next, we perform QPI measurements in a Ti-doped sample, $CsV_{3-x}Ti_xSb_5 (x = 0.15)$. Based on the doping-induced energy shifts of the Sb p_z band observed in both experiment and calculation (Figs. S6, S7 [46]), we utilize a CEC [Fig. 3(a)] with an energy 40 meV lower than the pristine counterpart as the FS of $CsV_{3-x}Ti_xSb_5 (x = 0.15)$. The FS consists of a Sb p_z band and V $3d$ bands, similar to those of CsV_3Sb_5. QPI simulations, orbital by orbital, are presented in Fig. 3(b). In experiments, the periodic density wave modulations and their corresponding wave vectors are completely suppressed (Fig. S8 [46]). Unlike the dominance of unidirectional coherent electronic states $\mathbf{q_2}$ and $\mathbf{q_3}$ in the low-energy QPI of the pristine sample, the

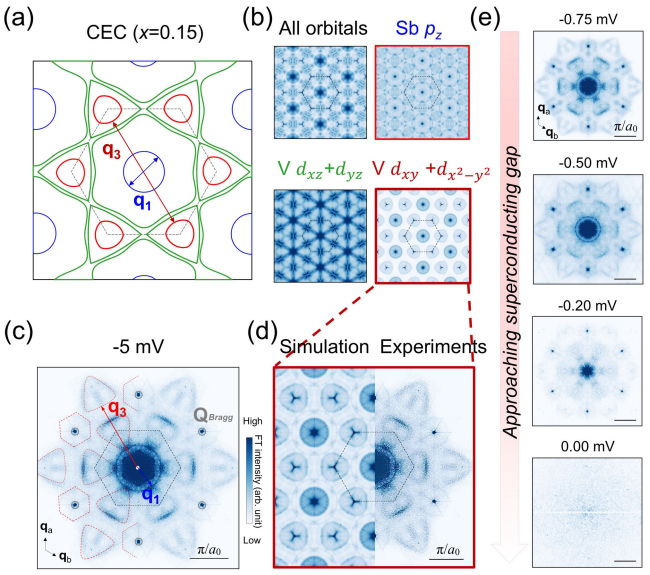

FIG. 3. (a) Calculated CEC at the Fermi surface of $CsV_{3-x}Ti_xSb_5 (x = 0.15)$. (b) The simulated QPI patterns based on all the orbitals, the Sb p_z orbital, the V d_{xz} and d_{yz} orbitals, and the V $d_{xy} + d_{x^2-y^2}$ orbitals in CEC of (a). (c) FT of dI/dV map in the normal state of $CsV_{3-x}Ti_xSb_5 (x = 0.15)$ at -5 mV. (d) The measured -5 mV QPI patterns (right) and the simulated Sb p_z orbitals and V $d_{xy} + d_{x^2-y^2}$ orbitals QPI pattern (left). (e) FT of dI/dV map in the superconducting state of $CsV_{3-x}Ti_xSb_5 (x = 0.15)$.

$dI/dV(\boldsymbol{q}, -5\ \mathrm{mV})$ reveals the dominant feature $\mathbf{q_3}$ [red dotted lines in Fig. 3(c)]. Surprisingly, only the QPI simulations from the interpocket and intrapocket scattering of in-plane V d_{xy} and $d_{x^2-y^2}$ orbitals centered around the K points align with the QPI patterns of the Ti-doped sample [Fig. 3(d)]. The dispersion of $\mathbf{q_3}$ matches DFT calculations, further confirming its origin from V d_{xy} and $d_{x^2-y^2}$ orbitals (Fig. S10 [46]). The QPI of Bogoliubov quasiparticles retains the overall patterns [Fig. 3(e)] but diminishes deep within the superconducting gap, reflecting the U-shaped superconducting gap with a depletion of the density of states. Intriguingly, the $\mathbf{q_1}$ scattering circle vanishes around −0.2 meV, while the $\mathbf{q_3}$ pattern remains detectable, indicating distinct orbital contributions to superconductivity in Ti-doped CsV_3Sb_5 (Fig. S11 [46]).

To track the evolution of V orbitals with Ti doping, QPI measurements on the Sb surfaces of $CsV_{3-x}Ti_xSb_5$ with varying concentrations are performed. The low-energy QPIs in lightly substituted samples ($x = 0.03, 0.04$), situated within the first superconducting dome, are primarily dominated by both $\mathbf{q_2}$ of V out-of-plane orbital and $\mathbf{q_3}$ of V in-plane orbitals [Fig. 4(a)], similar to the patterns observed in CsV_3Sb_5. With increasing x, the anisotropic stripe $\mathbf{q_3}$ weakens, while the scattering of V in-plane d_{xy} and $d_{x^2-y^2}$ orbitals $\mathbf{q_3}$ remains [right panel of Fig. 4(a)]. The highly substituted $CsV_{3-x}Ti_xSb_5 (x = 0.15, 0.27)$ transitions into the second superconducting dome. Apart from

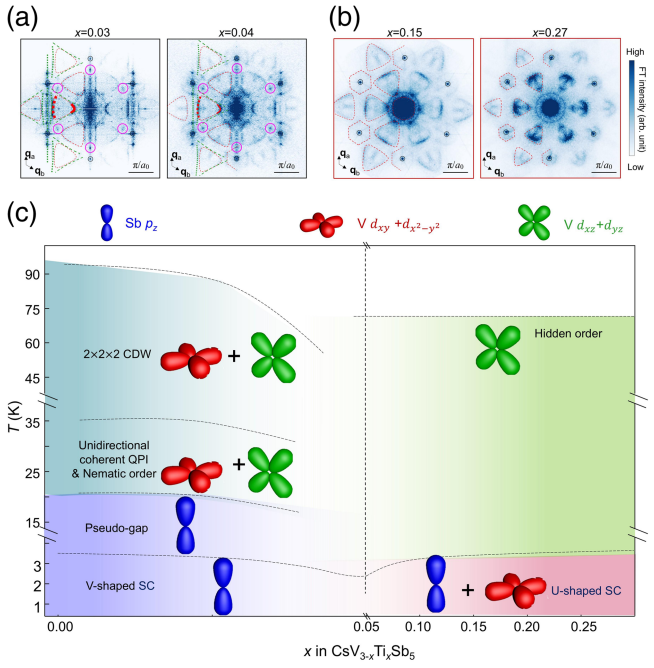

FIG. 4. (a) FTs of $dI/dV(\boldsymbol{r}, -5\ \mathrm{mV})$ map of $CsV_{3-x}Ti_xSb_5$, $x = 0.03,\ 0.04$. (b) FTs of $dI/dV(\boldsymbol{r}, -5\ \mathrm{mV})$ map of $CsV_{3-x}Ti_xSb_5$, $x = 0.15,\ 0.27$. (c) Schematic phase diagram of $CsV_{3-x}Ti_xSb_5$. The insets are the schematic of three orbitals correspond to each electronic phase based on QPI measurements.

$\mathbf{q_1}$ of the Sb p_z orbital, their QPIs are predominantly characterized by scattering vectors $\mathbf{q_3}$ from V in-plane orbitals [Fig. 4(b)]. Notably, the scattering vectors $\mathbf{q_2}$ from V out-of-plane orbitals are absent in the second superconducting phase without long-range CDWs.

In general, the segmented or hexagonal FSs (d_{xz} and d_{yz}) present stronger QPIs due to ideal nesting vectors ($\mathbf{q_2}$) and higher density of states in the kagome lattice. Thus, the promotion of smaller triangular FSs around the K points from d_{xy} and $d_{x^2-y^2}$ orbitals in QPIs by Ti doping is a striking feature. To gain a physical understanding, we performed a DFT calculation of the orbital resolved charge density redistribution due to the Ti substitution of a V atom in CsV_3Sb_5. When a V atom is replaced by a Ti atom, the charge modulations on the nearby V atoms show a clear pattern that involves primarily the in-plane d_{xy} and $d_{x^2-y^2}$ orbitals (Fig. S12 [46]). This indicates that the in-plane orbitals experience stronger scattering by the Ti dopants via the symmetry-allowed orbital hybridization than the out-of-plane d_{xz} and d_{yz} orbitals. This may account for the enhancement of the $\mathbf{q_3}$ QPI due to the Fermi pockets around the K points [Figs. 4(a) and 4(b)]. However, the disappearance of $\mathbf{q_2}$ from the out-of-plane orbitals scattering is puzzling, as Ti substitution of V suppresses the long-range CDWs and the gapped electrons of V d_{xz} and d_{yz} orbitals should be released. Our DFT calculations did not reveal any suppression of out-of-plane scattering from Ti impurities. Additionally, similar impurities on the Sb surface in Ti-doped samples (Fig. S13 [46]) should also be capable of scattering out-of-plane orbitals but were absent. This anomaly may be attributed to the hidden order that gaps the electrons [Fig. 1(e)] in the V d_{xz} and d_{yz} orbitals.

The orbital-dependent QPI patterns manifest distinct physics originating from different orbitals. In CsV_3Sb_5, the low-energy QPI of V out-of-plane and in-plane orbitals exhibits unidirectional patterns, suggesting that all the V d bands undergo an orbital-dependent renormalization, thereby playing significant roles in the nematic phase. However, the V out-of-plane and in-plane orbitals contribute differently to other exotic physics of the CsV_3Sb_5 system. With the suppression of CDWs, the QPI patterns of V out-of-plane orbitals disappear in the Ti-doped samples, while the hidden order remains, indicating that the hidden order is primarily contributed by the V out-of-plane orbitals. Regarding the SC states, the absence of an Sb p_z-orbital QPI inside the pseudogap and SC gap implies the participation of Sb p_z electrons in the formation of the pseudogap and therefore SC states in the pristine sample. Recent works [53,57,58] suggest an anisotropic SC gap in the V orbitals and an isotropic SC gap in the Sb orbital, further emphasizing the orbital-dependent SC states. In the Ti-doped sample, however, both Sb p_z orbital and V in-plane d orbital QPIs appear in the Bogoliubov QPI image, gapped by the U-shape SC gap successively, indicating a multiband superconductivity.

To summarize, we construct an orbital-resolved phase diagram of Ti-doped CsV_3Sb_5 with the Ti doping contents [Fig. 4(c)]. We map the Sb p_z orbital, V d_{xz} and d_{yz} orbitals, and V d_{xy} and $d_{x^2-y^2}$ orbitals onto different exotic electronic states based on QPI measurements. Notably, multiorbital physics is not limited to the AV_3Sb_5 family but are also prominent in other kagome materials, such as the orbital-selective electronic nematicity observed in ATi_3Bi_5 [59,60] (A = K, Rb, Cs) and ScV_6Sb_6 [61].

In conclusion, we have distinctively revealed the orbital origin of exotic electronic states in the kagome superconductor $CsV_{3-x}Ti_xSb_5$ through orbital-dependent QPI measurements across different Ti concentrations. These findings offer novel insights and avenues for exploring the crucial role of atomic orbitals in the cascade of symmetry-breaking correlated electronic states and superconductivity in kagome superconductors with broad implications in other quantum materials exhibiting multiorbital physics. Furthermore, doped CsV_3Sb_5 serves as a versatile platform for exploring exotic physics, with Cr dopants inducing magnetism [44,62], Mo dopants enhancing CDWs [63], and Ta dopants inducing orbital-dependent doping effects [64].

Acknowledgments—We are grateful to Wu Zhou, Junfeng He, Zhenyu Wang, and Lin Zhao for stimulating discussions. This work is supported by grants from the National Natural Science Foundation of China (62488201), the National Key Research and Development Projects of China (2022YFA1204100), and the CAS Project for Young Scientists in Basic Research (YSBR-003). B. Y. acknowledges the financial support by the Israel Science Foundation (ISF: 2932/21, 2974/23), German Research Foundation (DFG, CRC-183, A02), and by a research grant from the Estate of Gerald Alexander. Z. W. acknowledges the support of the U.S. Department of Energy (DOE), Basic Energy Sciences (BES). Grant No. DE-FG02-99ER45747 and Cottrell SEED Award No. 27856 from the Research Corporation for Science Advancement. F. L. acknowledges the support from the DOE-BES (Grant No. DE FG02-04ER46148).

[1] A. de la Torre, D. M. Kennes, M. Claassen, S. Gerber, J. W. McIver, and M. A. Sentef, Colloquium: Nonthermal pathways to ultrafast control in quantum materials, Rev. Mod. Phys. **93**, 041002 (2021).

[2] E. A. Stepanov, Eliminating orbital selectivity from the metal-insulator transition by strong magnetic fluctuations, Phys. Rev. Lett. **129**, 096404 (2022).

[3] F. B. Kugler and G. Kotliar, Is the orbital-selective Mott phase stable against interorbital hopping?, Phys. Rev. Lett. **129**, 096403 (2022).

[4] J. A. Sobota, Y. He, and Z.-X. Shen, Angle-resolved photoemission studies of quantum materials, Rev. Mod. Phys. **93**, 025006 (2021).

[5] H. Yoshida, J. Yamaura, M. Isobe, Y. Okamoto, G. J. Nilsen, and Z. Hiroi, Orbital switching in a frustrated magnet, Nat. Commun. **3**, 1 (2012).

[6] M. Yi, Y. Zhang, Z.-X. Shen, and D. Lu, Role of the orbital degree of freedom in iron-based superconductors, npj Quantum Mater. **2**, 57 (2017).

[7] D. N. Basov, R. D. Averitt, and D. Hsieh, Towards properties on demand in quantum materials, Nat. Mater. **16**, 11 (2017).

[8] M. Yi *et al.*, Observation of universal strong orbital-dependent correlation effects in iron chalcogenides, Nat. Commun. **6**, 1 (2015).

[9] A. Kostin, P. O. Sprau, A. Kreisel, Y. X. Chong, A. E. Böhmer, P. C. Canfield, P. J. Hirschfeld, B. M. Andersen, and J. C. S. Davis, Imaging orbital-selective quasiparticles in the Hund's metal state of FeSe, Nat. Mater. **17**, 10 (2018).

[10] R. Yu, J.-X. Zhu, and Q. Si, Orbital selectivity enhanced by nematic order in FeSe, Phys. Rev. Lett. **121**, 227003 (2018).

[11] H. Pfau *et al.*, Momentum dependence of the nematic order parameter in iron-based superconductors, Phys. Rev. Lett. **123**, 066402 (2019).

[12] M. Neupane, P. Richard, Z.-H. Pan, Y.-M. Xu, R. Jin, D. Mandrus, X. Dai, Z. Fang, Z. Wang, and H. Ding, Observation of a novel orbital selective Mott transition in $Ca_{1.8}Sr_{0.2}RuO_4$, Phys. Rev. Lett. **103**, 097001 (2009).

[13] P. O. Sprau, A. Kostin, A. Kreisel, A. E. Böhmer, V. Taufour, P. C. Canfield, S. Mukherjee, P. J. Hirschfeld, B. M. Andersen, and J. C. S. Davis, Discovery of orbital-selective Cooper pairing in FeSe, Science **357**, 75 (2017).

[14] Y. Hu *et al.*, Topological surface states and flat bands in the kagome superconductor CsV_3Sb_5, Sci. Bull. **67**, 495 (2022).

[15] B. R. Ortiz *et al.*, CsV_3Sb_5: A Z_2 Topological kagome metal with a superconducting ground state, Phys. Rev. Lett. **125**, 247002 (2020).

[16] B. R. Ortiz, P. M. Sarte, E. M. Kenney, M. J. Graf, S. M. L. Teicher, R. Seshadri, and S. D. Wilson, Superconductivity in the Z_2 kagome metal KV_3Sb_5, Phys. Rev. Mater. **5**, 034801 (2021).

[17] H. Li, H. Zhao, B. R. Ortiz, T. Park, M. Ye, L. Balents, Z. Wang, S. D. Wilson, and I. Zeljkovic, Rotation symmetry breaking in the normal state of a kagome superconductor KV_3Sb_5, Nat. Phys. **18**, 3 (2022).

[18] H. Zhao, H. Li, B. R. Ortiz, S. M. L. Teicher, T. Park, M. Ye, Z. Wang, L. Balents, S. D. Wilson, and I. Zeljkovic, Cascade of correlated electron states in the kagome superconductor CsV_3Sb_5, Nature (London) **599**, 7884 (2021).

[19] Z. Huang, X. Han, Z. Zhao, H. Yang, H. Chen, and H.-J. Gao, Formation and manipulation of diatomic rotors at the symmetry-breaking surfaces of a kagome superconductor, Nano Lett. **24**, 6023 (2024).

[20] H. Tan, Y. Liu, Z. Wang, and B. Yan, Charge density waves and electronic properties of superconducting kagome metals, Phys. Rev. Lett. **127**, 046401 (2021).

[21] Y.-X. Jiang *et al.*, Unconventional chiral charge order in kagome superconductor KV_3Sb_5, Nat. Mater. **20**, 10 (2021).

[22] C. Mielke *et al.*, Time-reversal symmetry-breaking charge order in a kagome superconductor, Nature (London) **602**, 7896 (2022).

[23] Y. Xu, Z. Ni, Y. Liu, B. R. Ortiz, Q. Deng, S. D. Wilson, B. Yan, L. Balents, and L. Wu, Three-state nematicity and

magneto-optical Kerr effect in the charge density waves in kagome superconductors, Nat. Phys. **18**, 12 (2022).
[24] L. Yu *et al.*, Evidence of a hidden flux phase in the topological kagome metal CsV_3Sb_5, arXiv:2107.10714.
[25] H. Chen *et al.*, Roton pair density wave in a strong-coupling kagome superconductor, Nature (London) **599**, 7884 (2021).
[26] L. Nie *et al.*, Charge-density-wave-driven electronic nematicity in a kagome superconductor, Nature (London) **604**, 7904 (2022).
[27] Y. Xiang, Q. Li, Y. Li, W. Xie, H. Yang, Z. Wang, Y. Yao, and H.-H. Wen, Twofold symmetry of c-axis resistivity in topological kagome superconductor CsV_3Sb_5 with in-plane rotating magnetic field, Nat. Commun. **12**, 1 (2021).
[28] H. Li, H. Zhao, B. R. Ortiz, Y. Oey, Z. Wang, S. D. Wilson, and I. Zeljkovic, Unidirectional coherent quasiparticles in the high-temperature rotational symmetry broken phase of AV_3Sb_5 kagome superconductors, Nat. Phys. **19**, 5 (2023).
[29] T. Neupert, M. M. Denner, J.-X. Yin, R. Thomale, and M. Z. Hasan, Charge order and superconductivity in kagome materials, Nat. Phys. **18**, 2 (2022).
[30] H. Chen, B. Hu, Y. Ye, H. Yang, and H.-J. Gao, Superconductivity and unconventional density waves in vanadium-based kagome materials AV_3Sb_5, Chin. Phys. B **31**, 097405 (2022).
[31] X. Mi, W. Xia, L. Zhang, Y. Gan, K. Yang, A. Wang, Y. Chai, Y. Guo, X. Zhou, and M. He, Multiband effects in thermoelectric and electrical transport properties of kagome superconductors $AV_3Sb_5(A = K, Rb, Cs)$, New J. Phys. **24**, 093021 (2022).
[32] H. Li *et al.*, Small fermi pockets intertwined with charge stripes and pair density wave order in a kagome superconductor, Phys. Rev. X **13**, 031030 (2023).
[33] D. Song *et al.*, Orbital ordering and fluctuations in a kagome superconductor CsV_3Sb_5, Sci. China Phys. Mech. Astron. **65**, 247462 (2022).
[34] K. Nakayama, Y. Li, T. Kato, M. Liu, Z. Wang, T. Takahashi, Y. Yao, and T. Sato, Carrier injection and manipulation of charge-density wave in kagome superconductor CsV_3Sb_5, Phys. Rev. X **12**, 011001 (2022).
[35] K. Nakayama, Y. Li, T. Kato, M. Liu, Z. Wang, T. Takahashi, Y. Yao, and T. Sato, Multiple energy scales and anisotropic energy gap in the charge-density-wave phase of the kagome superconductor CsV_3Sb_5, Phys. Rev. B **104**, L161112 (2021).
[36] H. Luo *et al.*, Electronic nature of charge density wave and electron-phonon coupling in kagome superconductor KV_3Sb_5, Nat. Commun. **13**, 1 (2022).
[37] M. Kang *et al.*, Twofold van Hove singularity and origin of charge order in topological kagome superconductor CsV_3Sb_5, Nat. Phys. **18**, 3 (2022).
[38] Y. Hu *et al.*, Rich nature of Van Hove singularities in Kagome superconductor CsV_3Sb_5, Nat. Commun. **13**, 1 (2022).
[39] H.-S. Xu, Y.-J. Yan, R. Yin, W. Xia, S. Fang, Z. Chen, Y. Li, W. Yang, Y. Guo, and D.-L. Feng, Multiband superconductivity with sign-preserving order parameter in kagome superconductor CsV_3Sb_5, Phys. Rev. Lett. **127**, 187004 (2021).
[40] Z. Huang *et al.*, Tunable vortex bound states in multiband CsV_3Sb_5-derived kagome superconductors, Sci. Bull. **69**, 885 (2024).
[41] A. A. Tsirlin, P. Fertey, B. R. Ortiz, B. Klis, V. Merkl, M. Dressel, S. D. Wilson, and E. Uykur, Role of Sb in the superconducting kagome metal CsV_3Sb_5 revealed by its anisotropic compression, SciPost Phys. **12**, 049 (2022).
[42] Y. M. Oey, B. R. Ortiz, F. Kaboudvand, J. Frassineti, E. Garcia, R. Cong, S. Sanna, V. F. Mitrović, R. Seshadri, and S. D. Wilson, Fermi level tuning and double-dome superconductivity in the kagome metal $CsV_3Sb_{5-x}Sn_x$, Phys. Rev. Mater. **6**, L041801 (2022).
[43] F. H. Yu, T. Wu, Z. Y. Wang, B. Lei, W. Z. Zhuo, J. J. Ying, and X. H. Chen, Concurrence of anomalous Hall effect and charge density wave in a superconducting topological kagome metal, Phys. Rev. B **104**, L041103 (2021).
[44] H. Yang *et al.*, Titanium doped kagome superconductor $CsV_{3-x}Ti_xSb_5$ and two distinct phases, Sci. Bull. **67**, 2176 (2022).
[45] Y. Zhong, Nodeless electron pairing in CsV_3Sb_5-derived kagome superconductors, Nature (London) **617**, 488 (2023).
[46] See Supplemental Material at http://link.aps.org/supplemental/10.1103/PhysRevLett.134.056001 for additional information on materials and methods and Figs. S1–S15, which includes Refs. [25,44,47–51].
[47] G. Kresse and J. Furthmüller, Efficiency of ab-initio total energy calculations for metals and semiconductors using a plane-wave basis set, Comput. Mater. Sci. **6**, 15 (1996).
[48] J. P. Perdew, K. Burke, and M. Ernzerhof, Generalized gradient approximation made simple, Phys. Rev. Lett. **77**, 3865 (1996).
[49] S. Grimme, J. Antony, S. Ehrlich, and H. Krieg, A consistent and accurate *ab initio* parametrization of density functional dispersion correction (DFT-D) for the 94 elements H-Pu, J. Chem. Phys. **132**, 154104 (2010).
[50] L. Bellaiche and D. Vanderbilt, Virtual crystal approximation revisited: Application to dielectric and piezoelectric properties of perovskites, Phys. Rev. B **61**, 7877 (2000).
[51] M. D. Johannes and I. I. Mazin, Fermi surface nesting and the origin of charge density waves in metals, Phys. Rev. B **77**, 165135 (2008).
[52] C. Wang *et al.* (private communications).
[53] H. Deng *et al.*, Chiral kagome superconductivity modulations with residual Fermi arcs, Nature (London) **632**, 775 (2024).
[54] Z. Liang *et al.*, Three-dimensional charge density wave and surface-dependent vortex-core states in a kagome superconductor CsV_3Sb_5, Phys. Rev. X **11**, 031026 (2021).
[55] B. Hu, Y. Ye, Z. Huang, X. Han, Z. Zhao, H. Yang, H. Chen, and H.-J. Gao, Robustness of the unidirectional stripe order in the kagome superconductor CsV_3Sb_5, Chin. Phys. B **31**, 058102 (2022).
[56] P. Wu *et al.*, Unidirectional electron–phonon coupling in the nematic state of a kagome superconductor, Nat. Phys. **19**, 1143 (2023).
[57] Y. Sun *et al.*, Imaging momentum-space Cooper pair formation and its competition with the charge density wave gap in a kagome superconductor, Sci. China Phys. Mech. Astron. **67**, 277411 (2024).

[58] A. Mine *et al.*, Direct observation of anisotropic Cooper pairing in kagome superconductor CsV_3Sb_5, arXiv:2404.18472.

[59] Y. Hu *et al.*, Non-trivial band topology and orbital-selective electronic nematicity in a titanium-based kagome superconductor, Nat. Phys. **19**, 1827 (2023).

[60] H. Yang *et al.*, Superconductivity and nematic order in a new titanium-based kagome metal $CsTi_3Bi_5$ without charge density wave order, Nat. Commun. **15**, 9626 (2024).

[61] Y.-X. Jiang *et al.*, Van Hove annihilation and nematic instability on a kagome lattice, Nat. Mater. **23**, 1214 (2024).

[62] G. Ding, H. Wo, Y. Gu, Y. Gu, and J. Zhao, Effect of chromium doping on superconductivity and charge density wave order in the kagome metal $Cs(V_{1-x}Cr_x)_3Sb_5$, Phys. Rev. B **106**, 235151 (2022).

[63] M. Liu, T. Han, X. Hu, Y. Tu, Z. Zhang, M. Long, X. Q. Hou, Mu, and L. Shan, Evolution of superconductivity and charge density wave through Ta and Mo doping in CsV_3Sb_5, Phys. Rev. B **106**, L140501 (2022).

[64] Y. Luo *et al.*, A unique van Hove singularity in kagome superconductor $CsV_{3-x}Ta_xSb_5$ with enhanced superconductivity, Nat. Commun. **14**, 3819 (2023).